

# A Spatio-temporal Attention-based Model for Infant Movement Assessment from Videos

Binh Nguyen-Thai, Vuong Le, Catherine Morgan, Nadia Badawi, Truyen Tran and Svetha Venkatesh

**Abstract**—The absence or abnormality of fidgety movements of joints or limbs is strongly indicative of cerebral palsy in infants. Developing computer-based methods for assessing infant movements in videos is pivotal for improved cerebral palsy screening. Most existing methods use appearance-based features and are thus sensitive to strong but irrelevant signals caused by background clutter or a moving camera. Moreover, these features are computed over the whole frame, thus they measure gross whole body movements rather than specific joint/limb motion.

Addressing these challenges, we develop and validate a new method for fidgety movement assessment from consumer-grade videos using human poses extracted from short clips. Human poses capture only relevant motion profiles of joints and limbs and are thus free from irrelevant appearance artifacts. The dynamics and coordination between joints are modeled using spatio-temporal graph convolutional networks. Frames and body parts that contain discriminative information about fidgety movements are selected through a spatio-temporal attention mechanism. We validate the proposed model on the cerebral palsy screening task using a real-life consumer-grade video dataset collected at an Australian hospital through the Cerebral Palsy Alliance, Australia. Our experiments show that the proposed method achieves the ROC-AUC score of 81.87%, significantly outperforming existing competing methods with better interpretability.

**Index Terms**—cerebral palsy, fidgety movement, infant movement assessment, general movements assessment, deep learning, spatio-temporal graph convolutional network, attention mechanism, human pose.

## I. INTRODUCTION

Cerebral palsy (CP) is the most common childhood physical disability impacting movement, posture, communication, and independence in daily activities [1]. CP occurs in up to 2.5/1000 live births in high-income countries and is estimated to affect 17 million people worldwide [2], [3]. The condition is

caused by abnormal development or damage in the developing brain. It is critical for an infant with CP to be diagnosed and receive intervention as early as possible [4]. Unfortunately, alarmingly high rates of children with CP are undiagnosed until later childhood due to the lack of awareness or expertise. A cheap and accurate assessment method is required.

Among early diagnostic methods of CP, the General Movements Assessment (GMA) has been found to be cost-effective and accurate [5]. Well-trained experts watch the videos of infants to identify the absence or abnormality of a particular movement pattern in a developmental state. A strong indicator for at-risk infants is the absence or sporadic occurrence of the so-called fidgety movements [6], [7]. Fidgety movements are small movements at moderate speed with variable acceleration of the neck, trunks, and limbs in all directions. Such movements typically occur in infants from approximately nine to twenty weeks post-term. Throughout this paper, we use the term “absent fidgety movements” or “absent fidgety” to refer to both cases: fidgety movements are totally absent or present sporadically with long pauses (sporadic fidgety movement) [7]. The main drawback of GMA is that it requires skilled experts and their time to study videos and provide the assessment. This makes the assessment inaccessible or delayed for many infants. Therefore, there is a need for tools that can automate the assessment of infant movements in videos.

Modeling the movements of joints and limbs in consumer-grade videos for fidgety movement assessment is challenging because: (i) The presence of irrelevant signals: such signals arise from irrelevant visual artifacts, e.g., illumination and background clutter; and camera properties. A moving camera can produce movement signals even when the infant does not move; a short distance from the camera to the infant will result in greater movement signals than from longer distances. (ii) Complex movement patterns: each joint not only has its movement patterns but also is influenced by other joints via the body structure. (iii) The irregularity of fidgety movements’ occurrences: fidgety movements may be stop-and-start. They occur at a joint at one time but may occur at another joint at another time. Overall, fidgety movements only occupy a small fraction of the whole body’s movement and are weak signals compared to other gross body movements.

Existing methods do not handle such complexity. Most current approaches use appearance-based features [8]–[12], and thus are sensitive to irrelevant appearance artifacts and camera properties. Therefore, the accuracies in those methods significantly degrade when applied to consumer-grade videos. Moreover, since features are calculated over the whole frames, they are indicative of gross measurement of the whole body

Binh Nguyen-Thai, Vuong Le, Truyen Tran and Svetha Venkatesh are with the Applied Artificial Intelligence Institute (A<sup>2</sup>I<sup>2</sup>), Deakin University, Waurn Ponds, VIC 3126, Australia (E-mail: b.nguyen@deakin.edu.au; vuong.le@deakin.edu.au; truyen.tran@deakin.edu.au; svetha.venkatesh@deakin.edu.au).

Catherine Morgan is with the Cerebral Palsy Alliance Research Institute, Specialty of Child & Adolescent Health, Sydney Medical School, Faculty of Medicine & Health, The University of Sydney, Sydney, NSW, Australia (Email: CMorgan@cerebralpalsy.org.au).

Nadia Badawi is with the Cerebral Palsy Alliance Research Institute, Specialty of Child & Adolescent Health, Sydney Medical School, Faculty of Medicine & Health, The University of Sydney, Sydney, NSW, Australia and also with the Grace Centre, The Children’s Hospital at Westmead, Sydney, NSW, Australia (Email: nadia.badawi@health.nsw.gov.au).

© 2021 IEEE. Personal use of this material is permitted. Permission from IEEE must be obtained for all other uses, in any current or future media, including reprinting/republishing this material for advertising or promotional purposes, creating new collective works, for resale or redistribution to servers or lists, or reuse of any copyrighted component of this work in other works. DOI: 10.1109/JBHI.2021.3077957.

movement, not that of joints and limbs.

In this work, we develop and validate a new method that addresses the aforementioned challenges for fidgety movement detection in consumer-grade videos. Our method works on human poses extracted from videos. A human pose can be represented as a time-series of 2D or 3D coordinates of body joint locations from which relevant motion features can be computed. Recent progress in pose estimation allows accurate extraction of 2D poses from videos. As human poses capture only the motion profiles of joints and limbs, our method eliminates the influence of irrelevant signals.

Given a video of an infant, we use a pose estimation algorithm to extract 2D poses from its frames and generate a pose sequence (see Section II-B). Our method takes this pose sequence as input and predicts the label of the infant.

In detail, we first split a pose sequence into a set of overlapping fixed-length windows, referred to as clips. This is motivated by the fact that fidgety movements occupy just a small fraction of the whole body's movement. Splitting a long sequence into clips will allow the model to extract useful movement patterns easier (see Fig.1 for an illustration). From each clip we construct a spatio-temporal pose graph and apply a spatio-temporal graph convolutional network (ST-GCN) [13], a model for spatio-temporal pose graph, to learn and represent the clip. We introduce a spatio-temporal attention mechanism on joints and clips that contain discriminative information about fidgety movements. As a result, the proposed method can focus on frames and body parts that contain meaningful movements, preventing them from being buried in the whole sequence. We term our method STAM, which stands for Spatio-temporal Attention-based Model.

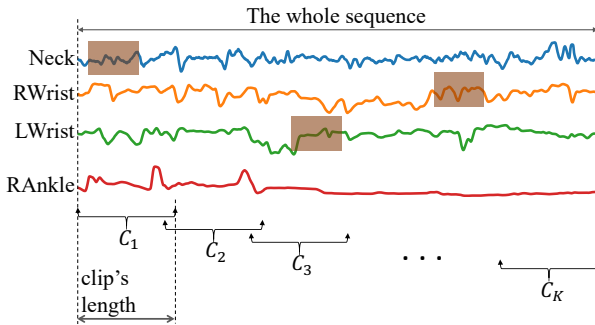


Fig. 1. A pose sequence split into overlapping clips. Brown rectangles are the places where fidgety movements happen.

We validate STAM on a dataset of 235 videos of infants who are at around 14-15 weeks post-term age collected at an Australian hospital. Our intensive suite of experiments shows that the proposed model significantly outperforms existing video-based CP diagnostic models with large margins.

In summary, the main contributions of this paper are:

- Design and implementation of a new framework for cerebral palsy detection from consumer-grade videos based on pose graph rather than appearance structure; and,
- Extensive experimentation on a real-life consumer-grade video dataset to confirm that the proposed model achieves better accuracy than existing baselines and is able to highlight key joints and clips.

The novelty in our framework includes: (i) a new Spatio-temporal graph convolutional network for clips with attention to joints, and (ii) a temporal attention mechanism for clips.

## II. PRELIMINARIES

### A. Fidgety movements

Fidgety movements (FMs) are movements of moderate speed and variable acceleration of the neck, trunks, and limbs in all directions. FMs are typically seen in infants from approximately 9 to 20 weeks post-term. The absence of FMs or presence of abnormal FMs are a strong predictor of adverse neurodevelopmental outcomes in infants. In particular, the absence of FM between 9-20 weeks is a strong predictor of cerebral palsy [6], [7].

FMs often co-occur with other gross movements such as kicking, wiggling—oscillating arm movements, or antigravity movements. The temporal organization of FMs can be divided into the following categories: (i) Continual FMs: FMs happen frequently but are interspersed with very short pauses, e.g., 1-2 seconds. FMs may be less obvious in the shoulders and wrists if the infant is focused on the environment. (ii) Intermittent FMs: The FMs are stop-and-start with longer pauses, e.g., 1-10 seconds. (iii) Sporadic FMs: when there are more gaps than bouts of fidgety (this is the same as absent FMs in infants between 11 and 16 weeks). (iv) Absent FMs: No FMs can be observed, although other movements may occur.

Thus, the occurrences of FMs are irregular in both spatial dimension (body parts) and temporal dimension (video frames) due to the interspersion of other movements. The detection of FMs is, therefore, a challenging task.

### B. Definitions

**Definition 1. Pose sequence.** The pose sequence of  $\tau$  consecutive video frames is defined as a set of  $M$  multi-variate time-series  $\{s_j\}_{j=1,M}$ . Here  $M$  is the number of body joints,  $s_j = [s_{j,1}, s_{j,2}, \dots, s_{j,\tau}]$  is a sequence of motion features of the  $j$ -th joint with  $s_{j,t} \in \mathbb{R}^c$  ( $t = 1, \tau$ ), where  $c$  is the dimensionality of the motion feature vector at each joint. The pose sequence is represented by a tensor  $S \in \mathbb{R}^{M \times c \times \tau}$ .

### C. Pose graph construction

Here we present how to construct the pose graph of a pose sequence  $S \in \mathbb{R}^{M \times c \times \tau}$ . The pose graph is denoted by  $G = (\mathcal{V}, \mathcal{E})$ , which consists of both intra-body and inter-frame connections. The node set  $\mathcal{V} = \{v_{j,t}\}$  ( $j = 1, M$ , and  $t = 1, \tau$ ) consists of  $M \times \tau$  nodes, where  $v_{j,t}$  correspond to the  $j$ -th joint at frame  $t$ . The feature vector of node  $v_{j,t}$  is  $S_{:,j,t} \in \mathbb{R}^c$ . The edge set  $\mathcal{E}$  consists of connections constructed as follows: intra-body connections are the limbs connecting joints according to human body structure, while inter-frame connections are the set of the links connecting each joint and itself on consecutive frames (see Fig.2).

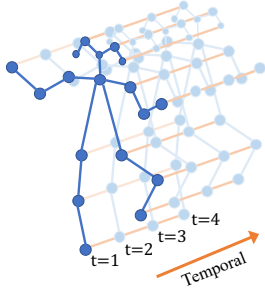


Fig. 2. Example of a pose graph. Blue lines are intra-body connections. Orange lines are inter-frame connections.

#### D. Spatial Graph Convolutional Networks

Graph convolutional networks generalize the convolutional neural networks (CNN) in grid data (e.g., images) to work on graph structure data [14]–[16]. In the conventional CNN on 2D images, the input of the convolutional operator is either an image or a feature map in a 2D grid, and the output feature map is also in a 2D grid. In contrast, a convolutional operator on graph takes node features and a graph structure as input and generates the node-level output features.

Convolutional graph networks can be applied to the pose graph in a single frame to capture the coordination of the joints. Here, we follow the Graph Convolutional Network (GCN) [16], a fast and simple version of graph convolutional networks. The layer-wise propagation rule is presented in Eq.1.

$$\mathbf{Z}^{(l+1)} = \sigma \left( \tilde{\mathbf{D}}^{-\frac{1}{2}} \tilde{\mathbf{A}} \tilde{\mathbf{D}}^{-\frac{1}{2}} \mathbf{Z}^{(l)} \mathbf{W}^{(l)} \right) \quad (1)$$

Here,  $\tilde{\mathbf{A}} = \mathbf{A} + \mathbf{I}_M$  is the adjacency matrix of an undirected graph  $G$  of  $M$  nodes with added self-connections.  $\mathbf{I}_M$  is the  $M \times M$  identity matrix,  $\tilde{\mathbf{D}}_{ii} = \sum_j \mathbf{A}_{ij}$  is the normalized degree matrix,  $\mathbf{W}^{(l)}$  a layer-specific learnable weight matrix.  $\mathbf{Z}^{(l+1)} \in \mathbb{R}^{M \times d_{l+1}}$  is the node feature map at the  $l$ -th layer;  $\mathbf{Z}^{(0)} \in \mathbb{R}^{M \times c}$  is the matrix of input node features. Function  $\sigma(\cdot)$  is a nonlinear activation function such as *ReLU*.

#### E. Spatial Temporal Graph Convolutional Networks

Spatial Temporal Graph Convolutional Networks (ST-GCN) [13] is a graph convolutional network which takes a pose graph as input and generates joint representations. Given a pose graph  $G$ , ST-GCN generates the node feature map  $\mathbf{Z} \in \mathbb{R}^{M \times d}$ . ST-GCN is used to capture both joint coordination and temporal patterns of the movements.

ST-GCN is a multi-layer neural network where each layer consists of two components: (i) a GCN which is applied to every single frame to capture the coordination of joints; and (ii) a temporal CNN, which is applied to the output of the GCN to capture the temporal patterns. The layer-wise propagation rule is as follows.

$$\mathbf{Z}^{(l+1)} = \text{Conv} \left( \left[ \mathbf{G}(\mathbf{Z}_1^{(l)}), \mathbf{G}(\mathbf{Z}_2^{(l)}), \dots, \mathbf{G}(\mathbf{Z}_{T_l}^{(l)}) \right] \right) + \text{Res} \quad (2)$$

Here  $\mathbf{Z}^{(l+1)} \in \mathbb{R}^{M \times d_{l+1} \times T_{l+1}}$  is the output feature map of the  $l$ -th layer;  $\mathbf{Z}_t^{(l)} \in \mathbb{R}^{M \times d_l}$  is the  $t$ -th frame of  $\mathbf{Z}^{(l)}$ ;  $\mathbf{G}(\mathbf{Z}_t^{(l)}) \in \mathbb{R}^{M \times d_{l+1}}$  is the feature map obtained by applying GCN to frame  $t$  of  $\mathbf{Z}^{(l)}$  (see Eq.1);  $\mathbf{Z}' \in \mathbb{R}^{M \times d_{l+1} \times T_l}$  is a

tensor obtained by stacking  $\mathbf{G}(\mathbf{Z}_t^{(l)})$  ( $t = \overline{1, T_l}$ ). Conv is the temporal CNN component which consists of a 2D CNN with kernel size  $= (t\_kernel, 1)$  and stride  $= (t\_stride, 1)$ . Res is a residual layer which is a 2D CNN with kernel size  $= (1, 1)$  and stride  $= (t\_stride, 1)$ . Here,  $t\_kernel$  and  $t\_stride$  are hyper-parameters specifying the temporal kernel size and temporal stride, respectively.

The output of the last layer,  $\mathbf{Z}^{(L)} \in \mathbb{R}^{M \times d \times T_L}$ , is fed to an average pooling over the third dimension ( $T_L$ ) to obtain the joint feature map  $\mathbf{Z} \in \mathbb{R}^{M \times d}$ .

### III. PROPOSED METHOD

#### A. Pipeline overview

The pipeline of our method is presented in Fig.3. First, we use a pose estimation algorithm to extract poses from video frames in the form of a set of time-series of 2D joint coordinates. Then we compute other motion features such as the velocities and accelerations of joints to form a pose sequence. These pose sequences are the input to STAM for training a classifier to predict the label of a pose sequence. We will detail the components.

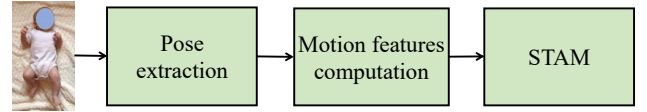


Fig. 3. Pipeline of the proposed method.

#### B. Pose extraction

**Pose estimation:** We used OpenPose [17], a pose estimation algorithm, to extract poses from video clips. OpenPose is a deep learning-based model that is trained on annotated image data to identify 2D positions of joints and limbs of humans in images. There are multiple options for the number of joints and the layouts of the pose to be extracted. In this work, we choose to use the layout with 18 joints, as presented in Fig.4. We include eyes and ears as they are relevant to the movements of the neck. By applying OpenPose, we estimated the positions of 18 joints for every frame.

OpenPose is originally trained using adult data, thus is suboptimal for infants due to the difference in body size and appearance. Therefore, retraining OpenPose using an annotated infant data is needed. This task was done in [18], with a pre-trained model provided. We use this pre-trained model for the pose estimation in our data.

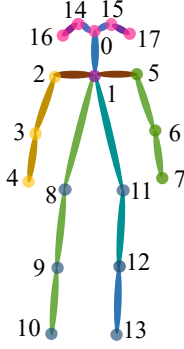


Fig. 4. Pose layout of a single frame. Joint indices: 0: nose, 1: neck, 2: right shoulder, 3: right elbow, 4: right wrist, 5: left shoulder, 6: left elbow, 7: left wrist, 8: right hip, 9: right knee, 10: right ankle, 11: left hip, 12: left knee, 13: left ankle, 14: right eye, 15: left eye, 16: right ear, 17: left ear.

**Preprocessing.** The estimated pose contained missing data (i.e., some joints are not detected) and outliers (e.g., background clutter that is inaccurately detected as joints). We perform a pre-processing process which includes: (i) *data imputation*: we imputed missing data using a linear interpolation to the raw time-series for each joint; (ii) *outlier removal*: we removed the outliers by using a rolling-median filter with a smoothing window of 0.5 seconds; and (iii) *signal smoothing*: we performed data smoothing by using a rolling-mean filter with a smoothing window of 0.5 seconds (see Fig.5).

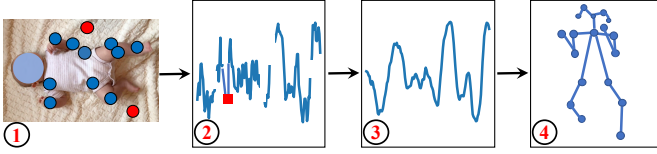


Fig. 5. Pipeline of the data pre-processing. (1) the input video with estimated joint locations (the dots). The data contains missing data (the right ankle, right wrist, left shoulder), outliers (red dots). (2) the time-series of joint coordinates with missing data (white space) and outlier (the red dot). (3) the time-series obtained after interpolating, removing outlier, and smoothing. (4) the pose obtained after standardizing.

In consumer-grade datasets, the videos are taken in various conditions such as camera viewpoints, distances from the camera to the infant. To remove the effect of these factors, we follow the process outlined in [18] to convert the poses to body-centered coordinates and normalize them to the same view and scale. The process includes: (i) rotating the upper body's joints around the center point of the shoulders; (ii) rotating the lower body's joints around the center point of the hips; and (iii) normalizing the body size using the trunk length (i.e., the distance between the neck and the center of the hips) as a reference distance: set the trunk length to 1 and translate the joint coordinates to get the ratios between the trunk length and the distances between joints to the neck remained (see Fig.5).

### C. Motion features computation

From the time-series of joint coordinates, we further compute other high-order motion features at each time step, which are important for modeling the motions. Those motion features

are the velocities, the accelerations, and the travel distances of joints at each frame. Velocities and accelerations are smoothed using a rolling-mean filter with a smoothing window of 0.25 seconds. The motion features of all frame will be stacked to form a pose sequence  $S \in \mathbb{R}^{M \times 7 \times T}$  of the video in which  $S_{j,:t} = [x_{j,t}, y_{j,t}, v_{j,t}^{(x)}, v_{j,t}^{(y)}, a_{j,t}^{(x)}, a_{j,t}^{(y)}, d_{j,t}]^T$  is the motion feature vector of the  $j$ -th joint at frame  $t$ . Here  $(x_{j,t}, y_{j,t})$  is the 2D coordinate;  $(v_{j,t}^{(x)}, v_{j,t}^{(y)})$  and  $(a_{j,t}^{(x)}, a_{j,t}^{(y)})$  are the velocities and accelerations over  $x$  and  $y$  axis; and  $d_{j,t}$  is the travel distance of the  $j$ -th joint at frame  $t$ .

### D. STAM: A Spatio-temporal Attention-based Model

Given the pose sequences extracted from the videos, we now proceed to construct our model to learn and represent the dynamics and coordinations of the joints and limbs for making predictions. We are given a set of sequence-label pairs  $\mathcal{D} = \{(S_i, y_i)\}_{i=1, \dots, N}$  of  $N$  videos, where  $S_i \in \mathbb{R}^{M \times c \times T}$  and  $y_i \in \{0, 1\}$  are the pose sequence and the label of the  $i$ -th video, respectively. Here  $y_i = 1$  if normal fidgety movements are present, and  $y_i = 0$  otherwise (e.g., cerebral palsy). We are interested in learning a classifier  $f : \mathbb{R}^{M \times c \times T} \rightarrow \{0, 1\}$  that predicts the label of an unseen pose sequence.

Our method, STAM, is motivated by the irregularity in the occurrences of fidgety movements (section II-A). Fidgety movements may occur at some joints in some consecutive video frames, however, the joints and frames are unknown. So we can break down a long sequence into overlapping clips (windows) where fidgety movements only occur at some joints in some of these clips. STAM will learn to select the joints and clips that contain discriminative information about fidgety movements. The high-level architecture of STAM is shown in Fig.6. Given the pose sequence  $S_i$ , we split it into  $K$  fixed-length clips  $(C_{i,1}, C_{i,2}, \dots, C_{i,K})$  where  $C_{i,k}$  ( $k = 1, \dots, K$ ) is a pose sequence of length  $w$ . From each  $C_{i,k}$ , we construct a pose graph using the procedure described in Section II-C, resulting in a set of  $K$  pose graphs  $(G_{i,1}, G_{i,2}, \dots, G_{i,K})$ . For simplicity, we omit the subscription  $i$  from the notations when no confusion arises, presenting a general infant. First, the pose graphs are fed to a Spatial Attention Graph Convolution Network (SAG), a component of STAM, which learns joint representations and aggregates them to generate clip-level representations, via a *spatial attention* mechanism. Then, clip-level representations are aggregated by a *temporal attention* mechanism to form the video-level representation, which will be used for the prediction.

**Spatial Attention Graph Convolutional Network (SAG).** We now detail SAG, a network that learns the representation of a pose graph with attention to joints. SAG is applied to clips for learning to generate clip-level representations. SAG extends ST-GCN (see Section II-E) with a spatial attention layer stacked on the top of the ST-GCN (see Fig.7). This layer generates the attention weights for joints and aggregates joint representations to obtain the clip-level representation.

In detail, a pose graph  $G_k$  ( $k = 1, \dots, K$ ) is first fed into a ST-GCN to generate joint representations  $\mathbf{z}_{k,j} \in \mathbb{R}^d$  ( $j = 1, \dots, M$ ).

$$\mathbf{z}_{k,1}, \mathbf{z}_{k,2}, \dots, \mathbf{z}_{k,M} = \text{ST-GCN}(G_k) \quad (3)$$

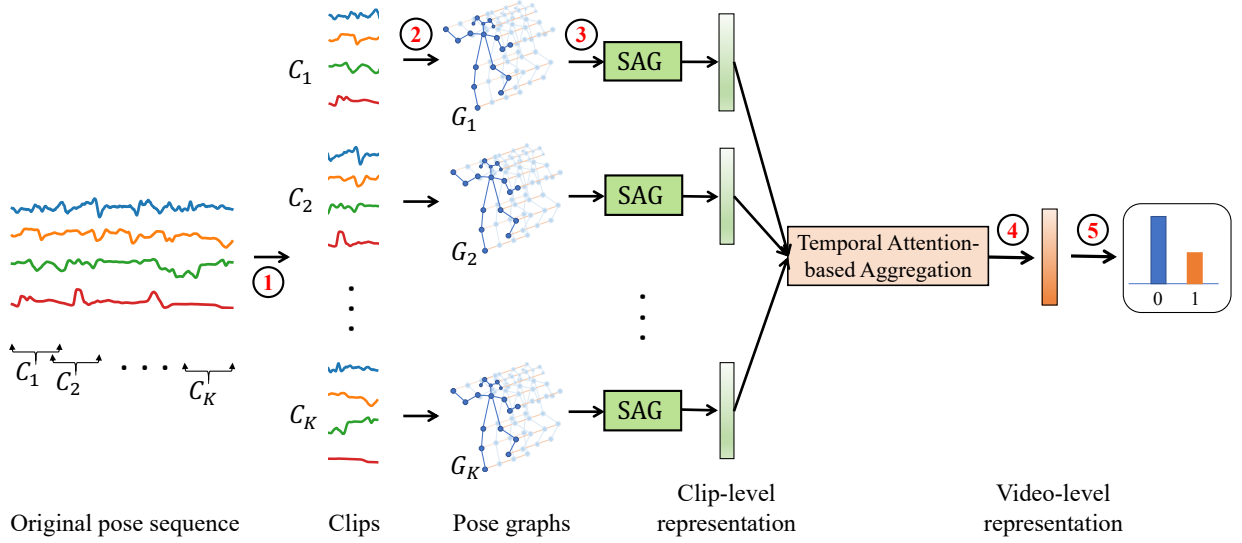


Fig. 6. High-level architecture of STAM. **Step 1**: split the pose sequence into overlapping clips. **Step 2**: construct the pose graph of each clip. **Step 3**: generate clip-level representations using Spatial Attention Graph Convolutional Network (SAG) (defined in Section III-D). **Step 4**: compute video-level representation using temporal attention. **Step 5**: make predictions.

Then, joint representations will be aggregated to obtain the clip-level representation. We propose to use the weighted average of the joint representations as the aggregation function, where the weights are generated by a neural network. Given a set of joint representations  $\{z_{k,1}, z_{k,2}, \dots, z_{k,M}\}$  of the  $k$ -th clip, we propose the following spatial attention-based aggregation function.

$$\mathbf{v}_k = \sum_{j=1}^M \beta_{k,j} \mathbf{z}_{k,j} \quad (4)$$

where the spatial attention weight  $\beta_{k,j}$  is calculated as follows:

$$\mathbf{u}_{k,j} = \tanh(\mathbf{W}_u \mathbf{z}_{k,j}) \quad (5)$$

$$\beta_{k,j} = \frac{\exp(\mathbf{w}_\beta^\top \mathbf{u}_{k,j})}{\sum_{j'} \exp(\mathbf{w}_\beta^\top \mathbf{u}_{k,j'})} \quad (6)$$

where  $\mathbf{W}_u \in \mathbb{R}^{d_u \times d}$  and  $\mathbf{w}_\beta \in \mathbb{R}^{d_u}$  are learnable parameters.

### Temporal attention-based aggregation.

Clip-level representations will be aggregated to obtain the video-level representation. We propose to use the weighted average of the clip-level representations as the aggregation function, where the weights are generated by a neural network. Given a set of clip-level representations  $\{\mathbf{v}_1, \mathbf{v}_2, \dots, \mathbf{v}_K\}$  of a pose sequence  $S$ , we propose the following temporal attention-based aggregation function.

$$\mathbf{c} = \sum_{k=1}^K \alpha_k \mathbf{v}_k \quad (7)$$

where the temporal attention weight  $\alpha_k$  is calculated as follows:

$$\mathbf{h}_k = \tanh(\mathbf{W}_h \mathbf{v}_k) \quad (8)$$

$$\alpha_k = \frac{\exp(\mathbf{w}_\alpha^\top \mathbf{h}_k)}{\sum_{k'} \exp(\mathbf{w}_\alpha^\top \mathbf{h}_{k'})} \quad (9)$$

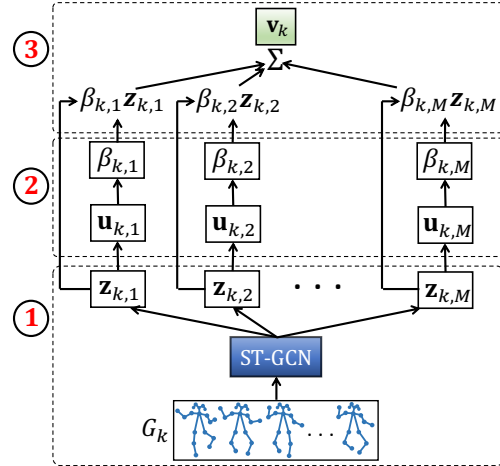


Fig. 7. Architecture of the Spatial Attention Graph Convolutional Network (SAG). **Step 1**: generate joint representations using ST-GCN, **Step 2**: generate spatial attention weights, **Step 3**: aggregate joints to compute the clip-level representation.

where  $\mathbf{W}_h \in \mathbb{R}^{d_h \times d}$  and  $\mathbf{w}_\alpha \in \mathbb{R}^{d_h}$  are learnable parameters.

**Prediction:** We use the video-level representation  $\mathbf{c}$  of the pose sequence  $S$  to predict the true class  $y = \{0, 1\}$  as follows:

$$\hat{y} = P(y = 1|S) = \sigma(\mathbf{w}^\top \mathbf{c} + b) \quad (10)$$

where  $\sigma(\cdot)$  is the sigmoid function,  $\mathbf{w} \in \mathbb{R}^d$  and  $b \in \mathbb{R}$  are learnable parameters.

**Loss function:** We use the cross-entropy loss as the objective function for learning the model parameters.

$$\mathcal{L}(\mathcal{D}) = -\frac{1}{N} \sum_{i=1}^N (y_i \log \hat{y}_i + (1 - y_i) \log(1 - \hat{y}_i)) \quad (11)$$

### E. Interpreting STAM

Here, we present a method to interpret the behavior of STAM by analyzing the attention weights. The availability of



attention weights at joint- and clip-level allows us to gain the insight about the contributions of joints at different segments of the video rather than only at the whole-sequence level.

We rewrite the Eq.(10) as follows.

$$\begin{aligned}
 P(y=1|S) &= \sigma \left( \mathbf{w}^\top \sum_{k=1}^K \alpha_k \mathbf{v}_k + b \right) \\
 &= \sigma \left( \mathbf{w}^\top \sum_{k=1}^K \alpha_k \sum_{j=1}^M \beta_{k,j} \mathbf{z}_{k,j} + b \right) \quad (12) \\
 &= \sigma \left( \sum_{k=1}^K \sum_{j=1}^M \alpha_k \beta_{k,j} \mathbf{w}^\top \mathbf{z}_{k,j} + b \right)
 \end{aligned}$$

Eq.(12) allows us to compute the contribution of each joint at each clip to the video's label. Specifically,  $\alpha_k \beta_{k,j} \mathbf{w}^\top \mathbf{z}_{k,j}$  can be interpreted as the contribution of the  $j$ -th joint at the  $k$ -th clip. Since  $\mathbf{w}$  is shared across the infants, we can omit  $\mathbf{w}$  and use  $\alpha_k \beta_{k,j}$  as the importance of the joints. We assume that high value of  $\alpha_k \beta_{k,j}$  should be assigned to the places (joints and clips) where fidgety movements occur.

#### IV. VALIDATION

##### A. Data

We used videos of 235 infants who are at around 14-15 weeks post-term age, provided by one hospital in Australia. Videos were taken as part of another study and were used with permission. These videos were primarily captured by parents using the BabyMoves App [19] via a smartphone in the infant's natural environment. Instructions for taking the video include using a plain background, having the infant lightly clothed and not sucking on a pacifier, or interacting with people or toys. Amongst the videos used for this analysis, there was considerable variability in lighting, background, the distance and orientation to the camera (camera view). The videos vary in resolution: 360x480 (147 videos), 480x360 (9 videos), 480x640 (3 videos), 480x720 (76 videos). The length of each video is approximately 4500 frames, equivalent to 2.5 minutes (30 frames per second). Of the videos used in this dataset, 200 were classified as normal fidgety, and the remaining 35 as absent fidgety.

##### B. Pose extraction

We extract the human pose using a pre-trained model for infant pose estimation [18]. The model was trained using a dataset of infant images with ground-truth labels of joint positions. Since this pre-trained model was carefully tuned on infant videos, we did not perform further evaluation on our dataset. Here we summarize the performance of the pose estimation based on the results reported in [18]. The performance of the pose estimation was evaluated using three metrics: (i) Root Mean Square Error (RMSE): the RMSE between the ground-truth joints and the estimated joints; (ii) Precision: the proportion of estimated joints that were present in the ground-truth joints; and (iii) Recall: the proportion of ground-truth points that are detected by the pose estimation algorithm. To

account for differences in scale, the RMSE is normalized by the size of the ground-truth bounding-box around the infant. As reported in [18], the RMSE in bounding-box unit is 0.02, the precision is 0.92, and the recall is 0.94. With this accuracy, the pre-trained model is applicable to extract joint positions in our infant videos.

##### C. Experimental settings

**Train/test split.** We split data into training and validation sets with ratio 8:2, using stratified random training/validation split. Stratified random split is used to retain the ratio of positive and negative examples in training and validation sets. To avoid the effect of data randomness, we perform re-shuffling and splitting 10 times, and report the average accuracy on the validation sets in all experiments. The number of positive (i.e., absent fidgety) and negative (i.e., normal fidgety) examples are: 28 positive and 160 negative examples for the training set; and 7 positive and 40 negative examples for the validation set.

**Voting based-prediction.** To increase the amount of data, we split each pose sequence into 4 sub-sequences using a sliding window with length 1000 frames and 200 overlapping frames, resulting in 112 positive and 640 negative examples for the training set and 28 positive and 160 negative examples for the validation set. The original sequence is considered positive if there exists one of its sub-sequences predicted as positive.

**Metrics.** We use Area Under the ROC Curve (ROC-AUC) of comparing  $\hat{y}_i$  with the true label  $y_i$  as the metric to evaluate the discrimination power of the proposed model. ROC-AUC is the most popular method to measure model's discrimination.

##### D. Baseline methods

We compare STAM with the following baselines:

- **MotionImage** [12]: This method uses appearance-based features. First, the videos are cropped to the smallest bounding boxes containing the infants. Then the motion images are calculated by subtracting consecutive frames. The quantity and the centroid of the motions are calculated from the motion images. Q-mean (mean of the quantity) and C-std (standard deviation of the centroid) of the motions are used as the scores for the classification.
- **Logistic Regression**: This is a logistic regression model which uses the feature vectors computed following [18] as input features. These features include the averages, medians, entropies, and deviations of the coordinates, velocities, accelerations. We normalize these feature vectors to zero-mean and unit-variance. The resulting vectors are used to train the logistic regression.
- **Conv2D-HOJD2D** [20]: This method applies a 2D convolutional neural network (Conv2D) to the Histogram of Joint Displacement 2D (HOJD2D) computed from human poses. The movement of each joint is represented by tracking its displacement at every frame. The displacements are organized into 16 bin histogram to form a feature vector in  $\mathbb{R}^{2 \times 16}$ . The feature vectors of 12 limb joints are stacked to form a HOJD2D matrix of size  $\mathbb{R}^{24 \times 16}$  which is used as the input of the Conv2D.

- **LSTM (Long-short term memory)**: To demonstrate the modeling power of STAM, we implement a baseline that uses the same pose sequence, without graph structure, as input. For this purpose, we use LSTM, which is standard for modeling sequential data. The input of this LSTM is a multivariate time-series of size  $\mathbb{R}^{7M \times T}$ , where each variable is a motion feature as described in Section III-C. Logistic regression is applied to the top hidden layer for predicting the label.
- **ST-GCN (Spatial Temporal Graph Convolutional Network)** [13]: This is a graph convolutional network for spatio-temporal data such as human pose.

#### E. Implementation details

For STAM, we use overlapping clips of length of 30 frames with 10 frames overlapping. We use a ST-GCN with three convolutional layers whose output channels are 64, 128, 256, respectively. Three convolutional layers use temporal kernel size  $t\_kernel = 9, 9, 9$  and temporal stride  $t\_stride = 1, 2, 2$ , respectively. We put a batch norm layer and a non-linear layer using *ReLU* function before the 2D CNN of the temporal CNN. We put a batch norm layer and a dropout layer with dropout rate=0.3 after the 2D CNN of the temporal CNN. The dimensionality of the clip-level representations and video-level presentation is  $d = 256$ . For Conv2D-HOJD2D, we use the architecture described in [20] with two convolutional layers. Each convolutional layer consists of a 2D convolutional layer with  $kernel\_size = 3$  and  $stride = 1$  followed by a max-pooling layer with  $kernel\_size = 3$  and a dropout layer with  $dropout\_rate = 0.3$ . For the LSTM, we use a network that consists of three hidden layers with dimensionality of 128. We use Adam [21] as the optimizer with learning rate  $lr = 0.0001$  and weight decay 0.0001 for all methods. We terminate the training after 800 epochs and report the results at the epoch giving the best validation accuracy. Source code is available at <https://github.com/nguyenthainh/stam>.

#### F. Result comparison

We report the ROC-AUC of all methods on Table I. As clearly seen, STAM significantly outperforms all competing methods. We also have the following observations.

TABLE I  
ROC-AUC OF STAM AND COMPETING METHODS. (\*): METHODS THAT USE APPEARANCE-BASED MOTION FEATURES.

Methods	ROC-AUC
MotionImage-Q-mean [12]*	0.5352 (0.0869)
MotionImage-C-std [12]*	0.5465 (0.0835)
Logistic Regression	0.6581 (0.1142)
Conv2D-HOJD2D [20]	0.6771 (0.0639)
LSTM	0.6925 (0.0341)
ST-GCN	0.7675 (0.0632)
STAM (proposed)	<b>0.8187</b> (0.0377)

(1) The pose features-based methods significantly outperform appearance features-based methods. This is expected because appearance-based features include irrelevant information as our dataset contains a lot of noise from background clutter and camera shakiness. This suggests that using

pose features is clearly better for consumer-grade videos. (2) Among pose features-based methods, Conv2D-HOJD2D, LSTM, and STAM significantly outperform Logistic Regression. This demonstrates the effectiveness of deep learning-based techniques in modeling the motions over just a simple model on hand-crafted features. (3) We observe the advantage of modeling the motion dynamics as LSTM, ST-GCN, and STAM outperform Conv2D-HOJD2D, which only captures the gross movements over the whole sequence. (4) The superiority of STAM and ST-GCN over LSTM confirms the advantage of taking into account the coordination of joints via graph structure. (5) The most encouraging result is that the proposed model STAM significantly outperforms ST-GCN. This confirms the effectiveness of the spatio-temporal attention mechanism which learns to focus on body parts and video frames that are meaningful for discriminating fidgety and non-fidgety movements.

#### G. ROC curve for practical use

We analyze the extent to which the proposed model can help practitioners in screening infants at risk. Fig. 8 shows the ROC curve, which presents the relationship between sensitivity and specificity. Based on this, end users can adjust the classification threshold to have the optimal sensitivity and specificity. For example, a threshold can be chosen to obtain a sensitivity of 80%, at a specificity of 62%.

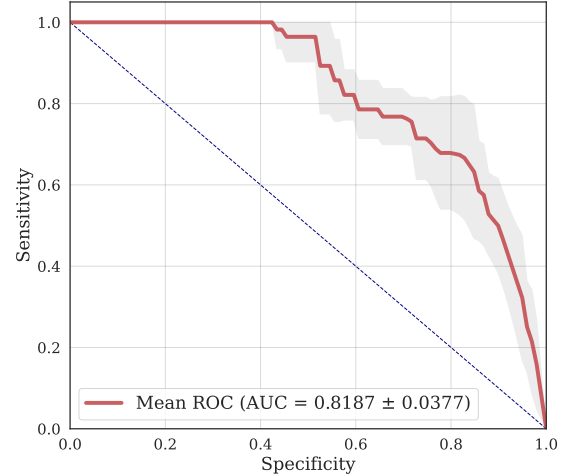


Fig. 8. ROC curve of the proposed model.

#### H. Qualitative analysis

To demonstrate the interpretability of the proposed attention mechanism, we present the attention weights of a healthy infant in Fig. 9. Here each row corresponds to a joint and each column corresponds to a clip. The value of cell  $(j, k)$  is  $\alpha_k \beta_{k,j}$  after being normalized to  $[0, 1]$ , and is expressed by the cell's color. The darker the red color, the higher the cell's value; the darker the blue color, the lower the cell's value, as shown in the color bar on the right of the grid. A high value of a cell indicates a high contribution of the corresponding joint and clip to the video's classification. To verify the behavior of

the attention weights, we asked an expert to annotate the places where fidgety movements happen. The cells corresponding to these places are marked with “×”. We can see that there is a substantial matching between the with highest values and “×” marker. Basically, high attention weights are assigned to the cells where fidgety movements occur (marked with “×”), while low attention weights are assigned to the cells where fidgety movements do not happen.

That observation confirms that the proposed model not only attains high predictive accuracy but also is able to highlight body parts and frames that contain discriminative information about fidgety movements.

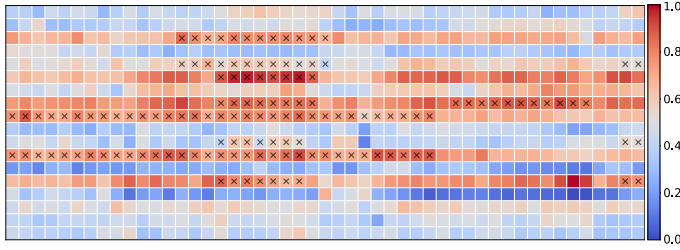


Fig. 9. Attention weights of a healthy infant. Each row corresponds to a joint where the row index follows the joint index presented in Fig.4. Each column corresponds to a clip where the column index is the clip’s index.

Fig.10 plots the video-level representations  $\mathbf{c}_i$  ( $i = \overline{1, N}$ ) using t-Distributed Stochastic Neighbor Embedding (t-SNE) [22]. We can see that most of the positive infants (orange dots) are well separated from normal infants (blue dots), showing the effectiveness of the proposed model in learning good discriminative representations.

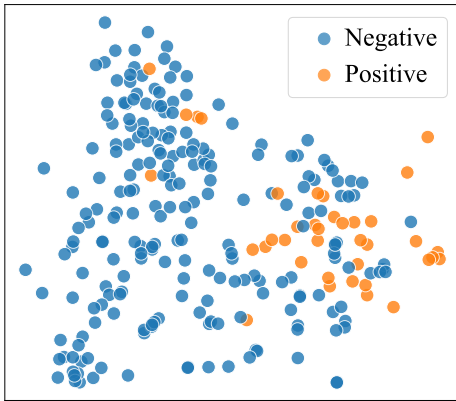


Fig. 10. Plot of the feature space using t-SNE.

### I. Ablation study

To gain more insight of the proposed model, we performed an ablation study by stripping STAM components. The results are reported in Table II. Overall, STAM-full (the the proposed model) outperforms its ablated variants, confirming the effectiveness of the proposed model. Details are as follows.

Model	ROC-AUC
STAM-full	<b>0.8187</b> (0.0377)
<b>Attention</b>	
STAM-w/o attention	0.7704 (0.0605)
STAM-w/ spatial attention	0.7853 (0.0641)
STAM-w/ temporal attention	0.7951 (0.0528)
<b>Clip modeling</b>	
LSTM-clip	0.7363 (0.0742)

TABLE II  
THE ACCURACIES OF STAM AND ITS SIMPLIFIED VARIANTS.

**Impact of the attention mechanism.** We study the following STAM variants: (i) STAM-w/o attention: a variant that does not use the attention mechanism. Clip-level representations are the means of the joint representations. The video-level representation is the mean of its clip representations; (ii) STAM-w/ spatial attention: a variant that uses only spatial attention. Clip-level representations are the weighted averages of the joint representations using spatial attention weights  $\beta_j$ . The video-level representation is the mean of its clip representations; and (iii) STAM-w/ temporal attention: a variant that uses only temporal attention. Clip-level representations are the means of the joint representations. The video-level representation is the weighted average of its clip representations using temporal attention weights  $\alpha_k$ .

We have the following observations: (1) Attention-based variants outperform non-attention variant. This result indicates that both spatial and temporal attention can add value in enhancing the predictive accuracy. (2) The improvement is amplified in STAM-full, when both spatial attention and temporal attention are used. This result confirms the superiority of STAM by selecting meaningful body parts and video frames simultaneously through the spatio-temporal attention.

**Impact of pose graph modeling.** We study LSTM-clip, a variant of STAM that replaces the SAG with a multi-variate LSTM. Each clip is modeled by an LSTM to generate the clip-level representation. The LSTM’s input is a multi-variate time-series which is exactly the same as the input of SAG, except the body graph structure.

The superiority of STAM confirms that modeling the pose graphs will handle the complexity of the movements better than considering the movements of joints independently.

### J. Time for the video assessment

After training, STAM can be used to assess an unseen infant’s video. The time needed to process and predict the video’s label is the sum of the time for: (i) human pose extraction from the video; (ii) preprocessing and motion feature computation; and (iii) label prediction. For a video of length 1000 frames (equivalent to 33 seconds), the total time needed is approximately 50 seconds (see Table III for the details).

TABLE III  
DETAILS OF THE TIME NEEDED TO ASSESS A VIDEO.

Step	Time (sec)
Human pose extraction	34
Motion feature computation	15
Label prediction	1
<b>Total</b>	<b>50</b>



## V. DISCUSSION

We have presented STAM, a method to identify infants at risk of cerebral palsy via video-based infant movement assessment. We extract human poses from the videos and model the movements of infants using a spatio-temporal graph neural network. We use a spatio-temporal attention mechanism to select body parts and video frames which contain discriminative features. STAM offers the following advantages over existing methods: (i) it operates on human poses extracted from videos, thus it is robust to irrelevant visual signals such as background clutter; (ii) it learns to extract meaningful motion features via spatio-temporal graph neural networks and the attention mechanism; and (iii) it provides a better interpretability through the spatial and temporal attention weights.

### A. Significance

This is the first time spatio-temporal graph convolutional networks and attention mechanisms are used with human pose sequences for cerebral palsy prediction. Since the human pose captures only the movements of joints and limbs, it is robust against irrelevant visual artifacts in videos. By normalizing the pose of every frame into the same view and scale, the method is independent of camera properties such as camera shakiness or camera angle. This allows the method to work well on consumer-grade videos. To verify the robustness of STAM, we exclude the videos captured in bad conditions from the test set and see whether the accuracy increases. The excluded videos are in one of the following cases: (i) the videos which contain background clutter, (ii) the videos which were captured by moving cameras, and (iii) the videos which were captured from side angles. We did not observe any significant change in the accuracy for all cases. In other words, including videos captured in bad conditions does not affect the model's accuracy.

In terms of modeling, by applying the spatio-temporal graph convolutional neural networks for modeling the movements, the proposed method can capture the complex motion dynamics of joints and limbs. The attention mechanism enables the model to amplify weak-but-important signals, prevent them from being buried in strong but irrelevant signals.

With those capabilities, the proposed method is expected to aid the cerebral palsy screening in many ways. First, it enables objective movement assessment. Judgment by humans may be subjective, so clinicians can cross-check with the result of our method to obtain objective decisions. Second, it can help reduce the specialist assessment burden and increase the number of infants that can be assessed as the method can process the videos taken at home by parents without the need of waiting to take the videos in the clinical environment. Finally, as our method uses human pose, it is a privacy-preserving technique, thus it enables data sharing between cohorts and hospitals for training the models without the risk that the infants are identified.

### B. Comparison to other works on infant movement assessment

**Wearable sensor-based methods.** Wearable sensors and 3D motion capture have been used to measure infant movements

[23]–[31]. Sensor-based measurements are objective and quantitative, and algorithms can generate risk assessments. However, these measurements have been restricted to laboratory and clinical settings, thus hindering the ability to evaluate infants in their natural environments. Moreover, sensor-based methods can be costly and time-intensive to develop and implement.

**Video-based methods.** Another line of methods for infant movement assessment is video-based. These methods use consecutive frame differencing to estimate movement features which are either the amount and centroid of motion [8]–[10] or optical flow [11], [12]. These features are used directly as scores or the input of a classifier. However, these pixel-based features are sensitive to irrelevant visual artifacts such as background clutter and illumination. Moreover, the features are extracted from the entire frame, over the whole sequence without focusing on meaningful body parts and frames.

**Human pose-based methods.** Recently, there have been several works that use human poses extracted from video clips. In [18], the authors extract infant poses from video clips then compute hand-crafted features such as velocities, accelerations, and entropies of the joints. They then compute the surprise score as the abnormal score for the movement. In [20], the authors proposed to use Histograms of Joint Orientation and Histograms of Joint Displacement. Those histogram features are used as the input of a convolutional neural network to train a movement classifier. However, since the features are calculated over the whole sequence, important frames and body parts are easy to be buried in the other part of the video. In addition, these methods cannot model the joint coordinations and dynamics of the movements.

### C. Limitations and future work

There still remains some limitations of the proposed method. First, STAM depends on the accuracy of the pose estimation algorithm, which may introduce noise or is sometimes inaccurate due to the occlusion of limbs. This can be addressed by fusing visual features guided by the human pose, e.g., the optical flow around joints and limbs. Second, since STAM is a supervised learning model, it needs annotated data which is usually hard to acquire. This can be solved by using self-supervised learning techniques to learn good representations from large datasets of unlabeled videos, e.g., learning to reconstruct masked joints.

## VI. CONCLUSION

We have developed and validated STAM, a new method for video-based infant movement assessment for cerebral palsy screening. The method uses human poses extracted from videos and is based on deep learning techniques using graph structures and spatio-temporal attention mechanisms. Experimental results confirm the competitive advantages of STAM on cerebral palsy screening. The key findings are: (i) Pose sequences are strong signals that retain motion information of joints and limbs whilst ignoring irrelevant, distracting visual artifacts; (ii) Representing pose sequences as spatial-temporal graphs and modeling the movements by spatial-temporal graph

convolutional networks work well as they capture the coordination and temporal patterns of joints and limbs; (iii) Attention mechanisms are useful for identifying discriminative patterns which are distributed over time and body parts.

**Ethical Approval:** The study was approved by the Mater Misericordiae Ltd Human Research Ethics Committee (MML HREC) (EC00332) in Australia (Review number: HREC/14/MHS/188).

## REFERENCES

- [1] I. Novak, C. Morgan, L. Adde, J. Blackman, R. N. Boyd, J. Brunstrom-Hernandez, G. Cioni, D. Damiano, J. Darrach, A.-C. Eliasson, L. S. de Vries, C. Einspieler, M. Fahey, D. Fehlings, D. M. Ferriero, L. Feters, S. Fiori, H. Forssberg, A. M. Gordon, S. Greaves, A. Guzzetta, M. Hadders-Algra, R. Harbourne, A. Kakooza-Mwesige, P. Karlsson, L. Krumlinde-Sundholm, B. Latal, A. Loughran-Fowlds, N. Maitre, S. McIntyre, G. Noritz, L. Pennington, D. M. Romeo, R. Shepherd, A. J. Spittle, M. Thornton, J. Valentine, K. Walker, R. White, and N. Badawi, "Early, Accurate Diagnosis and Early Intervention in Cerebral Palsy: Advances in Diagnosis and Treatment," *JAMA Pediatrics*, vol. 171, no. 9, pp. 897–907, 09 2017.
- [2] Australian Cerebral Palsy Register, "Australian Cerebral Palsy Register Report," no. December, p. 18, 2018. [Online]. Available: <https://cpregister.com/wp-content/uploads/2019/02/Report-of-the-Australian-Cerebral-Palsy-Register-Birth-Years-1995-2012.pdf>
- [3] C. Galea, S. McIntyre, H. Smithers-Sheedy, S. M. Reid, C. Gibson, M. Delacy, L. Watson, S. Goldsmith, N. Badawi, and E. Blair, "Cerebral palsy trends in Australia (1995–2009): a population-based observational study," *Developmental Medicine and Child Neurology*, vol. 61, no. 2, pp. 186–193, 2019.
- [4] C. Morgan, J. Darrach, A. M. Gordon, R. Harbourne, A. Spittle, R. Johnson, and L. Feters, "Effectiveness of motor interventions in infants with cerebral palsy: a systematic review," *Developmental Medicine & Child Neurology*, vol. 58, no. 9, pp. 900–909, 2016.
- [5] C. Einspieler, P. Marschik, A. Bos, F. Ferrari, G. Cioni, and H. Prechtel, "Early markers for cerebral palsy: Insights from the assessment of general movements," *Future Neurology*, vol. 7, no. 6, pp. 709–717, Nov. 2012.
- [6] C. Einspieler, R. Peharz, and P. B. Marschik, "Fidgety movements—tiny in appearance, but huge in impact," *Jornal de Pediatria*, vol. 92, no. 3, pp. S64–S70, 2016.
- [7] C. Einspieler, H. Yang, K. D. Bartl-Pokorny, X. Chi, F.-F. Zang, P. B. Marschik, A. Guzzetta, F. Ferrari, A. F. Bos, and G. Cioni, "Are sporadic fidgety movements as clinically relevant as is their absence?" *Early human development*, vol. 91, no. 4, pp. 247–252, 2015.
- [8] L. Adde, J. L. Helbostad, A. R. Jensenius, G. Taraldsen, K. H. Grunewaldt, and R. Støen, "Early prediction of cerebral palsy by computer-based video analysis of general movements: A feasibility study," *Developmental Medicine and Child Neurology*, vol. 52, no. 8, pp. 773–778, 2010.
- [9] L. Adde, J. L. Helbostad, A. R. Jensenius, G. Taraldsen, and R. Støen, "Using computer-based video analysis in the study of fidgety movements," *Early Human Development*, 2009.
- [10] A. Stahl, C. Schellewald, Ø. Stavdahl, O. M. Aamo, L. Adde, and H. Kirkerød, "An optical flow-based method to predict infantile cerebral palsy," *IEEE Transactions on Neural Systems and Rehabilitation Engineering*, vol. 20, no. 4, pp. 605–614, 2012.
- [11] H. Rahmati, O. M. Aamo, O. Stavdahl, R. Dragon, and L. Adde, "Video-based early cerebral palsy prediction using motion segmentation," in *IEEE Engineering in Medicine and Biology Society (EMBS)*, 2014, pp. 3779–3783.
- [12] R. Støen, N. T. Songstad, I. E. Silberg, T. Fjørtoft, A. R. Jensenius, and L. Adde, "Computer-based video analysis identifies infants with absence of fidgety movements," *Pediatric Research*, vol. 82, no. 4, pp. 665–670, oct 2017.
- [13] S. Yan, Y. Xiong, and D. Lin, "Spatial temporal graph convolutional networks for skeleton-based action recognition," in *AAAI Conference on Artificial Intelligence*, 2018.
- [14] M. Defferrard, X. Bresson, and P. Vandergheynst, "Convolutional neural networks on graphs with fast localized spectral filtering," in *Advances in neural information processing systems (NIPS)*, 2016, pp. 3844–3852.
- [15] J. B. Estrach, W. Zaremba, A. Szlam, and Y. LeCun, "Spectral networks and deep locally connected networks on graphs," in *International Conference on Learning Representations (ICLR)*, 2014.
- [16] T. N. Kipf and M. Welling, "Semi-supervised classification with graph convolutional networks," in *International Conference on Learning Representations (ICLR)*, 2017.
- [17] Z. Cao, T. Simon, S. Wei, and Y. Sheikh, "Realtime multi-person 2d pose estimation using part affinity fields," in *IEEE Conference on Computer Vision and Pattern Recognition (CVPR)*, 2017, pp. 1302–1310.
- [18] C. Chambers, N. Seethapathi, R. Saluja, H. Loeb, S. Pierce, D. Bogen, L. Prosser, M. J. Johnson, and K. P. Kording, "Computer vision to automatically assess infant neuromotor risk," *IEEE Transactions on Neural Systems and Rehabilitation Engineering*, vol. 28, no. 11, pp. 2431–2442, 2020.
- [19] A. K. Kwong, A. L. Eeles, J. E. Olsen, J. L. Cheong, L. W. Doyle, and A. J. Spittle, "The baby moves smartphone app for general movements assessment: Engagement amongst extremely preterm and term-born infants in a state-wide geographical study," *Journal of paediatrics and child health*, vol. 55, no. 5, pp. 548–554, 2019.
- [20] K. D. McCay, E. S. Ho, H. P. Shum, G. Fehringer, C. Marcroft, and N. D. Embleton, "Abnormal Infant Movements Classification with Deep Learning on Pose-Based Features," *IEEE Access*, vol. 8, pp. 51 582–51 592, 2020.
- [21] D. P. Kingma and J. Ba, "Adam: A method for stochastic optimization," in *International Conference on Learning Representations (ICLR)*, 2015.
- [22] L. Van der Maaten and G. Hinton, "Visualizing data using t-sne," *Journal of machine learning research*, vol. 9, no. 11, 2008.
- [23] M. Fan, D. Gravem, D. M. Cooper, and D. J. Patterson, "Augmenting gesture recognition with erlang-cox models to identify neurological disorders in premature babies," in *ACM Conference on Ubiquitous Computing (UbiComp)*, 2012, pp. 411–420.
- [24] F. Heinze, K. Hesels, N. Breitbach-Faller, T. Schmitz-Rode, and C. Disselhorst-Klug, "Movement analysis by accelerometry of newborns and infants for the early detection of movement disorders due to infantile cerebral palsy," *Medical and Biological Engineering and Computing*, vol. 48, no. 8, pp. 765–772, 2010.
- [25] N. Kanemaru, H. Watanabe, H. Kihara, H. Nakano, T. Nakamura, J. Nakano, G. Taga, and Y. Konishi, "Jerky spontaneous movements at term age in preterm infants who later developed cerebral palsy," *Early Human Development*, vol. 90, no. 8, pp. 387–392, 2014.
- [26] D. Karch, K. S. Kang, K. Wochner, H. Philippi, M. Hadders-Algra, J. Pietz, and H. Dickhaus, "Kinematic assessment of stereotypy in spontaneous movements in infants," *Gait and Posture*, vol. 36, no. 2, pp. 307–311, 2012.
- [27] D. Karch, K. S. Kim, K. Wochner, J. Pietz, H. Dickhaus, and H. Philippi, "Quantification of the segmental kinematics of spontaneous infant movements," *Journal of Biomechanics*, vol. 41, no. 13, pp. 2860–2867, 2008.
- [28] H. Philippi, D. Karch, K. S. Kang, K. Wochner, J. Pietz, H. Dickhaus, and M. Hadders-Algra, "Computer-based analysis of general movements reveals stereotypies predicting cerebral palsy," *Developmental Medicine and Child Neurology*, vol. 56, no. 10, pp. 960–967, 2014.
- [29] H. Rahmati, H. Martens, O. M. Aamo, O. Stavdahl, R. Stoen, and L. Adde, "Frequency analysis and feature reduction method for prediction of cerebral palsy in young infants," *IEEE Transactions on Neural Systems and Rehabilitation Engineering*, vol. 24, no. 11, pp. 1225–1234, 2016.
- [30] C. B. Redd, L. A. Barber, R. N. Boyd, M. Varnfield, and M. K. Karunanithi, "Development of a Wearable Sensor Network for Quantification of Infant General Movements for the Diagnosis of Cerebral Palsy," *IEEE Engineering in Medicine and Biology Society (EMBS)*, pp. 7134–7139, 2019.
- [31] M. Singh and D. J. Patterson, "Involuntary gesture recognition for predicting cerebral palsy in high-risk infants," in *International Symposium on Wearable Computers (ISWC)*, 2010.